Breast Cancer (2019) 26:113–124
https://doi.org/10.1007/s12282-018-0899-8

ORIGINAL ARTICLE

Histogram analysis of quantitative pharmacokinetic parameters on DCE-MRI: correlations with prognostic factors and molecular subtypes in breast cancer

Ken Nagasaka[1] · Hiroko Satake[1] · Satoko Ishigaki[1] · Hisashi Kawai[1] · Shinji Naganawa[1]

Received: 24 April 2018 / Accepted: 26 July 2018 / Published online: 1 August 2018

Abstract

Background Breast cancer heterogeneity influences poor prognoses thorough therapy resistance. This study quantitatively evaluated intratumoral heterogeneity through a histogram analysis of dynamic contrast-enhanced MRI (DCE-MRI) pharmacokinetic parameters, and determined correlations with prognostic factors and molecular subtypes.

Methods We retrospectively investigated 101 invasive ductal breast cancers from 99 women who underwent preoperative DCE-MRI between July 2012 and November 2014. Pharmacokinetic parameters (K^{trans}, k_{ep}, and v_e) were obtained by the Tofts model. For each parameter, the mean, standard deviation, coefficient of variation, skewness, and kurtosis values of tumor were calculated, and prognostic factors and subtypes associations were assessed.

Results The mean of v_e was lower in cancers with high Ki-67 than in cancers with low Ki-67 ($P = 0.002$). The coefficient of variation of v_e was higher in cancers with estrogen receptor negativity than in cancers with estrogen receptor positivity ($P < 0.001$). The coefficient of variation of v_e was also higher in cancers with high Ki-67 than in cancers with low Ki-67 ($P < 0.001$). The skewness of v_e was higher in cancers with high nuclear grade than in cancers with low nuclear grade ($P = 0.006$). Triple-negative cancers showed higher v_e coefficient of variation than did those with luminal A ($P < 0.001$) and B ($P = 0.006$).

Conclusions Various v_e parameters correlated with breast cancer prognostic factors and molecular subtypes.

Keywords Brest cancer · Dynamic contrast-enhanced MRI · Histogram analysis · Pharmacokinetic modeling

Introductions

Angiogenesis is known to play a central role in the growth and metastasis of malignant tumors [1–3]. One challenging goal for radiologists is to noninvasively assess tumor microvascular physiology, in addition to the conventional morphological imaging diagnoses. With respect to breast imaging, dynamic contrast-enhanced MRI (DCE-MRI) is the most popular method for evaluating vascular function, and it is able to quantify tumor perfusion, permeability, and the extravascular extracellular space (EES) volume. Three quantitative pharmacokinetic parameters are representative of, and commonly used for, the pharmacokinetic analysis of breast cancer imaging with DCE-MRI: K^{trans} (the transfer constant of the contrast agent from the plasma compartment into the EES), k_{ep} (the rate constant of the escape of the contrast agent from the EES into the plasma compartment), and v_e (the EES per unit volume of tissue). Several studies that have investigated breast DCE-MRI have reported that these parameters are not only useful for differentiating between benign and malignant tumors [4, 5] but are also associated with breast cancer prognostic factors [6–8] and responses to neoadjuvant chemotherapy [9].

On the other hand, breast cancers are heterogeneous, on both genetic and histopathological levels, with intratumoral spatial variation, and breast cancer intratumoral heterogeneity has been considered to be a factor related to poor prognosis, owing to resistance to therapy. Intratumoral heterogeneity is caused by variations of the tumor microenvironment, including angiogenesis, cell density, immune cell infiltration, extracellular matrix remodeling, and other changes [10–12].

✉ Ken Nagasaka
ken-nagasaka@med.nagoya-u.ac.jp

[1] Department of Radiology, Nagoya University Graduate School of Medicine, 65 Tsurumai-cho, Shouwa-ku, Nagoya 466-8550, Japan

Because of the developments in breast cancer imaging techniques, spatial heterogeneity can be quantitatively depicted by various analyses. In histogram analyses of diffusion-weighted imaging (DWI), the apparent diffusion coefficient (ADC) value distributions have quantitatively shown greater heterogeneity in triple-negative breast cancer (TNBC) than in hormone receptor-positive subtypes [13]. In breast cancer neoadjuvant chemotherapy, ADC histogram analysis has been reported to quantitatively show alterations during treatment courses [14]. In computerized texture analyses, breast cancers with more heterogeneity on T2-weighted images and less heterogeneity on contrast-enhanced T1-weighted subtraction images are correlated with poorer survival [15]. With regard to quantitative pharmacokinetic analysis of breast DCE-MRI, a recent publication has shown that the quantification of intratumoral heterogeneity, using histogram analyses, can improve the diagnostic accuracy in differentiating between benign and malignant lesions [16].

In this study, we have quantitatively evaluated intratumoral heterogeneity in breast cancers through a histogram analysis of DCE-MRI pharmacokinetic parameters, which are correlated with prognostic factors and molecular subtypes.

Materials and methods

Study patients

The Ethics Committee of our hospital approved this study, and the requirement for informed patient consent was waived.

A retrospective search of the breast image database at our institution identified 211 female patients with breast cancer who underwent DCE-MRI on a 3-T clinical MRI system, for preoperative evaluations, from July 2012 through November 2014. Among these patients, women who were not treated at our hospital ($n=7$), received preoperative chemotherapy ($n=22$), or were diagnosed with ductal carcinoma in situ (DCIS) ($n=53$) or special types of breast cancer ($n=14$) were excluded. Lesions that presented non-mass-like enhancements ($n=10$) were also excluded. Contralateral tumors were evaluated separately, as individual cancers. When multiple ipsilateral breast masses existed, we evaluated the largest one. There was no pathological evidence of independent multiple tumor origin. Thus, 101 invasive ductal breast cancers from 99 patients were statistically analyzed in our study.

MRI acquisition

Bilateral breast MRI was performed using the 3-T clinical MRI system (MAGNETOM Skyra; Siemens Healthcare, Erlangen, Germany), with a 16-channel breast array coil, in the prone position. Following routine T2-weighted imaging with fat saturation and diffusion-weighted imaging, 3D gradient echo sequences with volumetric interpolated breath-hold examination (VIBE) at different flip angles, 2° and 20°, were acquired for T1 mapping with following parameters: repetition time/echo time (TR/TE) = 7.5/3 ms, field of view = 340 × 340 mm, matrix = 224 × 168, number of slices = 176, slice thickness = 0.9 mm, and acquisition time = 1 min and 2 s. Next, DCE-MRI was performed using time-resolved angiography with interleaved stochastic trajectories (TWIST) sequence and the following parameters: TR/TE = 7.2/3.8 ms, flip angle = 15°, field of view = 340 × 340 mm, matrix = 448 × 336, number of slices = 176, slice thickness = 0.9 mm, and no gap. Water excitation for fat suppression and a parallel imaging technique that used generalized autocalibrating partially parallel acquisitions (GRAPPA) acceleration factor of 3 were also applied. The A% and B% values of the TWIST sequence were set at 32 and 20%, respectively. The A% is the size of central k-space region A, which is always filled completely during TWIST acquisition, and the B% is the sampling density of peripheral region B, in each repetition. The acquisition time for the first TWIST DCE-MRI frame (full k-space sampling) was 2 min and 10 s, whereas those for the rest of the frames were 1 min. The total DCE-MRI acquisition time was 8 min and 10 s. At the beginning of the third DCE-MRI frame acquisition, gadolinium-based contrast agents, gadopentetate dimeglumine (Magnevist; Bayer Yakuhin, Osaka, Japan), gadodiamide (Omniscan; Daiichi Sankyo, Tokyo, Japan), or gadoterate meglumine (Magnescope; Guerbet, Tokyo, Japan) were administered intravenously, at 0.1 mmol/kg and a flow rate of 2 mL/s, using a power injector, followed by a 20-mL saline flush. T1 mapping and DCE-MRI were performed in the axial plane, and bilateral breast images were acquired.

Image analysis

The enhancement kinetics were analyzed using commercially available software (Tissue 4D; Siemens Healthcare) on the basis of the two-compartment Tofts model [17]. The intermediate model arterial input function (AIF), which was based on a mathematical simulation and was provided by the software, was used for the analysis in all the cases. K^{trans}, k_{ep}, and v_e were calculated pixel-by-pixel. These pharmacokinetic parameters are related by the equation: $k_{ep} = K^{trans}/v_e$. For measurement of the pharmacokinetic parameters of the tumor, a freehand region of interest (ROI) was drawn along the contour of the tumor, on the slice with maximum diameter, on the last-phase postcontrast images after motion correction and registration of morphological and precontrast data to the dynamic series. ROIs were selected

by one radiologist with 23 years of experience in interpreting breast images. Pixel-wise pharmacokinetic parameter maps of K^{trans}, k_{ep}, and v_e were created, and the ROIs were copied to the same spatial position. To eliminate necrotic changes and non-physiological values, all pixels included in K^{trans}, with values equal to 0 min^{-1} or above 4 min^{-1}, and k_{ep}, with values equal to 0 min^{-1} or above 40 min^{-1}, were excluded. Similarly, voxels with v_e equal to 0 or above 1 were excluded. The mean and standard deviation values of each parameter within the ROIs were obtained. Furthermore, to assess heterogeneity, the coefficient of variation, skewness, and kurtosis values of each parameter within the ROIs were calculated.

Histopathologic assessment

The expression statuses of estrogen receptor (ER), progesterone receptor (PR), human epidermal growth factor receptor 2 (HER2), and Ki-67 were obtained from histopathologic reports of surgical specimens. The ER and PR expression statuses were, respectively, scored according to the Allred scoring system, with proportion scores (PS, ranging 0–5), intensity scores (IS, ranging 0–3), and total scores (TS = PS + IS, ranging 0, 2–8). ER expression was considered as positive if TS was greater than or equal to three. PR expression was considered as positive if PS was greater than two. HER2 expression was scored as 0, 1+, 2+, or 3+, on the basis of immunohistochemical staining. Tumors with a score of 3+ were considered as HER2-positive, and tumors with a score of 0 or 1+ were considered as HER2-negative. In tumors with a score of 2+, gene amplification, using fluorescence in situ hybridization, was used to determine the HER2 status. HER2 expression was considered as positive if the ratios of HER2 gene copies to chromosome 17 signals were greater than 2. Molecular subtypes were defined based on the St. Gallen consensus, as follows: luminal A (positive for ER and/or PR, with Ki-67 < 15%); luminal B (positive for ER and/or PR, with overexpressed HER2 or Ki-67 ≥ 15%); HER2 (negative for ER and PR, with overexpressed HER2); triple-negative (negative for ER, PR, and HER2 receptors).

Statistical analysis

All cases were dichotomized into two groups according to pathologic prognostic factors: expression of ER, PR, and HER2 (positive vs, negative); tumor size (> 20 mm vs, ≤ 20 mm, corresponding to pathological stage T2 and more, or T1); Ki-67 index (> 20% vs, ≤ 20%); nuclear grade (grade 2 or 3 vs, grade 1); axillary lymph-node status (positive vs, negative). The perfusion parameters (K^{trans}, k_{ep}, and v_e) were compared with the pathologic prognostic factors using the Mann–Whitney U test and with the molecular subtypes (luminal A, luminal B, and triple-negative) using the Kruskal–Wallis test, followed by the Steel–Dwass multiple comparison test. Because of our small population size of patients with HER2-type breast cancer, we limited our analyses to comparisons between luminal A, luminal B, and triple-negative subtypes. The Bonferroni correction was applied across the comparison with prognostic factors, to counteract the multiple testing problem, for statistics of pharmacokinetic parameter separately. P values less than 0.05/7 = 0.0071, for the comparison with prognostic factors, and P values less than 0.05, for the comparison with subtypes, were considered statistically significant. All statistical analyses were performed using the R statistical package (http://www.r-project.org).

Results

Among total 101 breast cancers, ER positive versus negative were 82 (81.2%) versus 19 (18.8%), PR positive versus negative were 61 (60.4%) versus 40 (39.6%), HER2 negative versus positive were 90 (89.1%) versus 11 (10.9%), Ki-67 > 20% versus ≤ 20% were 42 (41.6%) versus 57 (56.4%), nuclear grade 2 or 3 versus 1 were 72 (71.3%) versus 28 (27.8%), and invasive diameter > 20 mm versus ≤ 20 mm were 26 (25.7%) versus 74 (73.4%). We could not obtain two cancer statuses in Ki-67, and one cancer status in nuclear grade and invasive diameter. These missing values were excluded from analysis.

The correlations between K^{trans} and pathologic prognostic factors are summarized in Table 1. In comparison between invasive diameters greater than 20 mm and less or equal to 20 mm, the P values of kurtosis and skewness were less than 0.05; however, after the Bonferroni correction, no significant differences were found between various K^{trans} values according to pathologic prognostic factors.

The correlations between k_{ep} and pathologic prognostic factors are summarized in Table 2. No significant differences were found between various k_{ep} values according to pathologic prognostic factors.

The correlations between v_e and pathologic prognostic factors are shown in Table 3. The mean values of v_e were significantly higher in cancers with low Ki-67 expression than in cancers with high Ki-67 expression ($P = 0.002$). The coefficients of variation values of v_e were significantly higher in cancers with ER negativity than in cancers with ER positivity ($P < 0.001$). The coefficients of variation values of v_e were also significantly higher in cancers with high Ki-67 expression than in cancers with low Ki-67 expression ($P < 0.001$). The skewness values of v_e were significantly higher in cancers with high nuclear grade than in cancers with low nuclear grade ($P = 0.006$).

Of the 101 invasive ductal breast cancers, 44 (43.6%) were classified as luminal A, 38 (37.6%) as luminal B, 14

Table 1 Correlation between K^{trans} and pathologic prognostic factors

	Mean (min^{-1})	*P*	SD (min^{-1})	*P*	CV	*P*	Kurtosis	*P*	Skewness	*P*
ER		0.089		0.608		0.313		0.696		0.965
Positive	0.295 (0.245–0.401)		0.186 (0.137–0.320)		0.630 (0.462–0.879)		9.812 (1.907–25.230)		2.696 (1.030–4.421)	
Negative	0.265 (0.204–0.300)		0.184 (0.143–0.224)		0.708 (0.496–1.056)		12.036 (3.307–19.826)		3.396 (1.302–3.985)	
PR		0.167		0.972		0.130		0.324		0.417
Positive	0.302 (0.237–0.412)		0.185 (0.871–0.324)		0.573 (0.439–0.871)		9.544 (1.122–24.472)		2.516 (0.895–0.895)	
Negative	0.271 (0.226–0.351)		0.190 (0.145–0.256)		0.688 (0.500–0.922)		11.939 (3.856–22.398)		3.281 (1.531–4.118)	
HER2		0.616		0.695		0.601		0.316		0.366
Positive	0.295 (0.269–0.269)		0.177 (0.152–0.199)		0.570 (0.480–0.757)		11.843 (2.945–46.978)		3.450 (1.228–5.322)	
Negative	0.280 (0.227–0.392)		0.196 (0.134–0.302)		0.645 (0.487–0.895)		10.135 (2.294–23.278)		2.732 (0.981–4.156)	
Ki-67		0.120		0.590		0.515		0.173		0.275
> 20%	0.266 (0.209–0.345)		0.184 (0.150–0.226)		0.651 (0.534–0.878)		15.720 (3.458–27.847)		3.555 (1.553–4.258)	
≤ 20%	0.302 (0.246–0.396)		0.186 (0.133–0.333)		0.624 (0.469–0.904)		7.358 (1.896–23.802)		2.651 (0.956–4.381)	
Nuclear grade		0.091		0.070		0.240		0.345		0.730
High (2 or 3)	0.271 (0.224–0.363)		0.178 (0.136–0.246)		0.596 (0.458–0.879)		11.939 (2.960–26.388)		2.894 (1.173–4.546)	
Low (1)	0.321 (0.254–0.445)		0.221 (0.157–0.394)		0.720 (0.522–0.937)		8.657 (1.650–21.730)		2.599 (0.933–4.155)	
Invasive diameter		0.443		0.975		0.129		**0.015**		**0.018**
> 20 mm	0.264 (0.205–0.303)		0.192 (0.162–0.241)		0.654 (0.557–0.902)		17.575 (7.698–39.164)		3.896 (1.914–4.839)	
≤ 20 mm	0.305 (0.250–0.406)		0.186 (0.128–0.325)		0.581 (0.447–0.880)		7.080 (1.842–21.607)		2.456 (0.908–4.057)	
LN metastasis		0.073		0.259		0.741		0.724		1.000
Positive	0.260 (0.208–0.334)		0.181 (0.114–0.247)		0.639 (0.503–0.874)		13.820 (2.077–25.137)		3.653 (1.073–4.229)	
Negative	0.294 (0.253–0.411)		0.189 (0.149–0.313)		0.623 (0.468–0.924)		9.812 (2.580–24.049)		2.696 (1.070–4.394)	

Data are presented as median (interquartile range). *P* values were derived from the Mann–Whitney *U* test. *P* values < 0.05 are presented in bold

ER estrogen receptor, *PR* progesterone receptor, *HER2* human epidermal growth factor receptor 2, *LN* lymph node, *SD* standard deviation, *CV* coefficient of variation

Table 2 Correlation between k_{ep} and pathologic prognostic factors

	Mean (min^{-1})	*P*	SD (min^{-1})	*P*	CV	*P*	Kurtosis	*P*	Skewness	*P*
ER		0.907		0.838		0.764		0.512		0.373
Positive	0.867 (0.739–1.047)		0.550 (0.427–0.736)		0.648 (0.495–0.760)		7.062 (1.445–14.235)		2.277 (1.040–3.076)	
Negative	0.876 (0.765–0.975)		0.568 (0.445–0.758)		0.630 (0.484–0.827)		3.846 (2.394–9.283)		1.794 (1.127–2.672)	
PR		0.925		0.376		0.431		0.881		0.931
Positive	0.852 (0.723–1.051)		0.537 (0.422–0.735)		0.646 (0.486–0.753)		6.520 (0.843–0.843)		2.234 (0.765–3.172)	
Negative	0.873 (0.761–0.984)		0.600 (0.454–0.743)		0.642 (0.512–0.823)		5.961 (2.143–11.751)		2.139 (1.213–2.915)	
HER2		0.777		0.130		0.156		0.844		0.499
Positive	0.819 (0.790–1.019)		0.479 (0.415–0.540)		0.535 (0.477–0.607)		6.634 (2.159–14.242)		1.869 (1.165–2.585)	
Negative	0.871 (0.735–1.017)		0.592 (0.437–0.754)		0.657 (0.495–0.816)		5.986 (1.496–13.267)		2.240 (1.036–3.053)	
Ki-67		0.112		0.430		0.902		0.667		0.808
> 20%	0.919 (0.802–1.072)		0.601 (0.456–0.711)		0.630 (0.512–0.744)		6.356 (2.527–13.514)		2.052 (1.275–2.823)	
≤ 20%	0.834 (0.715–1.006)		0.541 (0.420–0.748)		0.652 (0.493–0.817)		6.521 (1.162–13.645)		2.309 (0.827–3.103)	
Nuclear grade		0.744		0.648		0.284		0.209		0.665
High (2 or 3)	0.869 (0.767–1.011)		0.550 (0.437–0.700)		0.611 (0.493–0.776)		6.356 (1.792–15.414)		2.254 (1.061–3.092)	
Low (1)	0.852 (0.699–1.056)		0.602 (0.405–0.763)		0.707 (0.519–0.798)		5.157 (0.546–9.113)		2.240 (0.719–2.918)	
Invasive diameter		0.120		0.610		0.370		0.052		0.120
> 20 mm	0.802 (0.683–0.976)		0.538 (0.439–0.649)		0.642 (0.540–0.867)		9.121 (2.709–16.291)		2.519 (1.424–3.222)	
≤ 20 mm	0.874 (0.739–1.066)		0.582 (0.423–0.756)		0.648 (0.478–0.756)		5.408 (0.895–11.635)		2.074 (0.796–2.927)	
LN metastasis		0.118		0.279		0.969		0.730		0.707
Positive	0.787 (0.714–0.968)		0.540 (0.415–0.658)		0.652 (0.524–0.744)		10.318 (0.558–14.708)		2.516 (0.674–3.208)	
Negative	0.902 (0.766–1.033)		0.579 (0.440–0.754)		0.644 (0.492–0.808)		5.870 (1.913–12.723)		2.217 (1.066–1.066)	

Data are presented as median (interquartile range). *P* values were derived from the Mann–Whitney *U* test

ER estrogen receptor, *PR* progesterone receptor, *HER2* human epidermal growth factor receptor 2, *LN* lymph node, *SD* standard deviation, *CV* coefficient of variation

Table 3 Correlation between v_e and pathologic prognostic factors

	Mean	*P*	SD	*P*	CV	*P*	Kurtosis	*P*	Skewness	*P*
ER		0.066		**0.016**		**< 0.001***		0.091		**0.018**
Positive	0.403 (0.301–0.476)		0.130 (0.109–0.152)		0.326 (0.273–0.383)		1.021 (0.153–3.207)		0.776 (0.395–1.359)	
Negative	0.343 (0.286–0.402)		0.143 (0.135–0.162)		0.412 (0.359–0.513)		3.556 (0.715–4.195)		1.426 (0.869–1.638)	
PR		0.258		**0.047**		**0.015**		0.723		0.598
Positive	0.398 (0.307–0.474)		0.130 (0.108–0.150)		0.329 (0.278–0.376)		1.023 (0.174–3.834)		0.835 (0.427–1.447)	
Negative	0.372 (0.290–0.452)		0.141 (0.123–0.162)		0.387 (0.299–0.446)		1.195 (0.357–3.699)		1.032 (0.452–1.527)	
HER2		0.844		0.271		0.571		0.819		0.371
Positive	0.398 (0.353–0.424)		0.143 (0.134–0.152)		0.361 (0.323–0.387)		1.199 (0.838–2.313)		1.137 (0.977–1.315)	
Negative	0.383 (0.299–0.474)		0.134 (0.111–0.152)		0.336 (0.285–0.413)		1.062 (0.176–3.884)		0.825 (0.409–1.586)	
Ki-67		**0.002***		0.527		**< 0.001***		0.072		**0.049**
> 20%	0.333 (0.270–0.402)		0.138 (0.117–0.154)		0.411 (0.337–0.478)		2.688 (0.520–4.334)		1.403 (0.616–1.710)	
≤ 20%	0.416 (0.330–0.480)		0.136 (0.110–0.153)		0.323 (0.279–0.377)		1.019 (0.178–2.823)		0.769 (0.400–1.325)	
Nuclear grade		**0.048**		0.794		**0.014**		**0.020**		**0.006***
High (2 or 3)	0.346 (0.293–0.446)		0.134 (0.114–0.153)		0.357 (0.295–0.436)		1.569 (0.203–4.157)		1.111 (0.551–1.679)	
Low (1)	0.427 (0.377–0.473)		0.138 (0.106–0.152)		0.315 (0.263–0.348)		0.632 (0.069–1.516)		0.631 (0.277–0.950)	
Invasive diameter		0.358		0.700		0.671		**0.013**		**0.012**
> 20 mm	0.346 (0.287–0.452)		0.134 (0.116–0.148)		0.322 (0.291–0.414)		3.448 (0.895–4.710)		1.389 (0.904–1.713)	
≤ 20 mm	0.400 (0.308–0.472)		0.136 (0.109–0.155)		0.345 (0.274–0.404)		0.855 (0.153–2.655)		0.749 (0.409–1.331)	
LN metastasis		0.293		0.326		0.927		0.121		0.147
Positive	0.342 (0.284–0.442)		0.125 (0.113–0.148)		0.339 (0.304–0.402)		1.199 (0.652–5.330)		1.137 (0.552–1.812)	
Negative	0.406 (0.314–0.471)		0.139 (0.113–0.153)		0.343 (0.278–0.407)		1.021 (0.183–3.488)		0.825 (0.415–1.421)	

*P values < 0.0071 were considered statistically significant after the Bonferroni correction

Data are presented as median (interquartile range). P values were derived from the Mann–Whitney U test. P values < 0.05 are presented in bold

ER estrogen receptor, *PR* progesterone receptor, *HER2* human epidermal growth factor receptor 2, *LN* lymph node, *SD* standard deviation, *CV* coefficient of variation

(13.9%) as triple-negative, and 5 (4.9%) as HER2. The K^{trans} and k_{ep} values showed no significant differences among tumor subtypes (Figs. 1, 2). The Kruskal–Wallis test indicated that there was significant difference in the coefficient of variation values of v_e between luminal A, luminal B, and triple-negative subtypes ($P < 0.001$) (Fig. 3). The post hoc Steel–Dwass test for multiple comparisons revealed that the coefficient of variation values of v_e in triple-negative were significantly higher than those in the luminal A and luminal B subtypes ($P < 0.001$ and $P = 0.006$, respectively). The mean of v_e tended to be lower, and the kurtosis and skewness values of v_e tended to be higher, in triple-negative cancers than in luminal-type cancers, although these differences were not statistically significant. Pharmacokinetic parameter maps and corresponding histograms of two representative cases are compared in Fig. 4a, b. One is a luminal A type cancer which shows higher mean but lower coefficient of variation, kurtosis, and skewness values of v_e. The other case is a triple-negative cancer which shows lower mean but higher coefficient of variation, kurtosis, and skewness values of v_e.

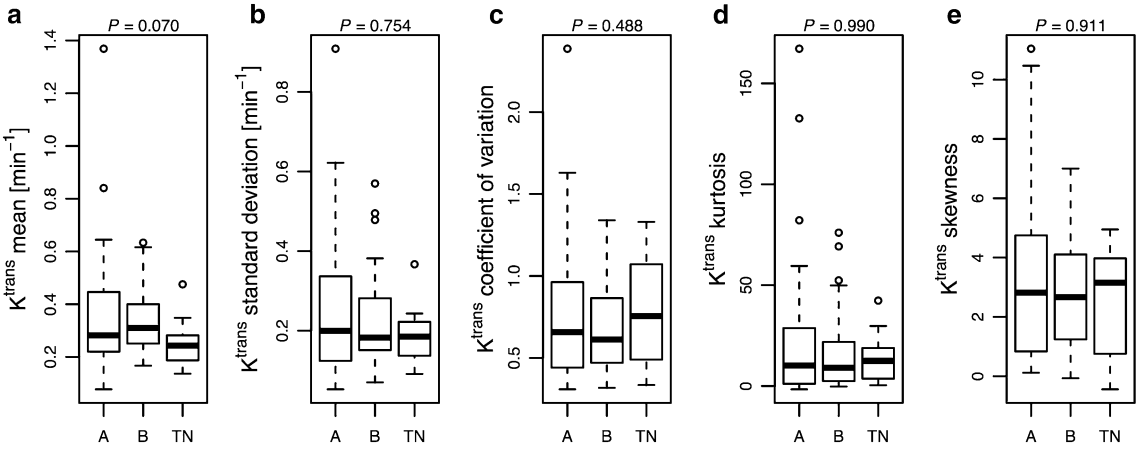

Fig. 1 Boxplots of the **a** median, **b** standard deviation, **c** coefficient of variation, **d** kurtosis, and **e** skewness values of K^{trans} according to luminal A, luminal B, and triple-negative. *A* luminal A, *B* luminal B, *TN* triple-negative. The boxes show the median with the upper and lower quartiles. The whiskers indicate the minimal value within a 1.5 interquartile range (IQR) of the lower quartile, and the maximum value within a 1.5 IQR of the upper quartile. The open circles indicate the outliers. The *P* values above each plot were calculated with the Kruskal–Wallis test

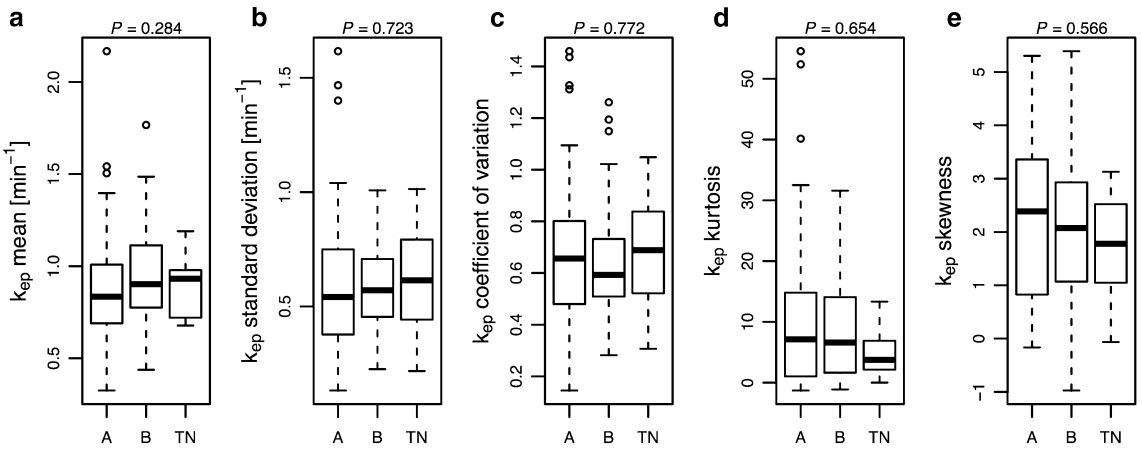

Fig. 2 Boxplots of the **a** median, **b** standard deviation, **c** coefficient of variation, **d** kurtosis, and **e** skewness values of k_{ep} according to luminal A, luminal B, and triple-negative. *A* luminal A, *B* luminal B, *TN* triple-negative. The boxes show the median with the upper and lower quartiles. The whiskers indicate the minimal value within a 1.5 interquartile range (IQR) of the lower quartile, and the maximum value within a 1.5 IQR of the upper quartile. The open circles indicate the outliers. The *P* values above each plot were calculated with the Kruskal–Wallis test

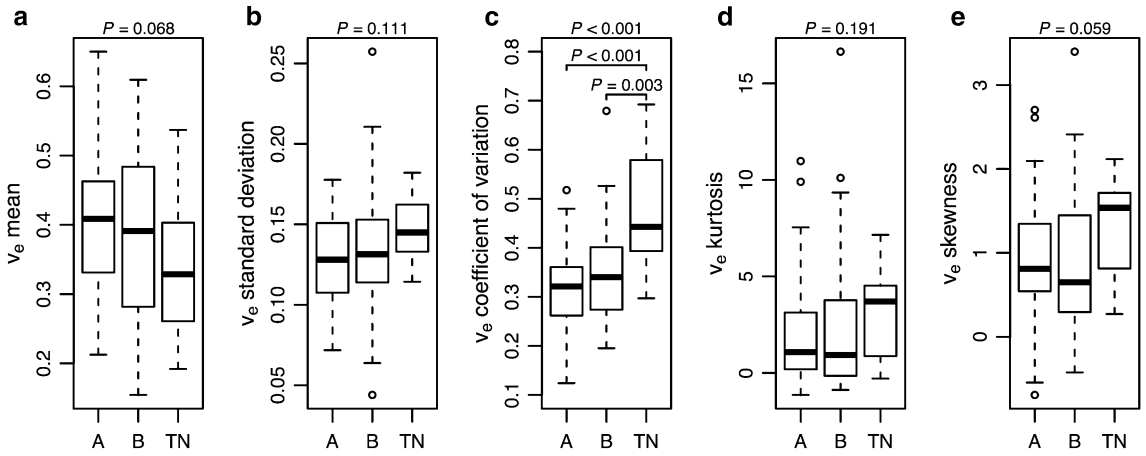

Fig. 3 Boxplots of the **a** median, **b** standard deviation, **c** coefficient of variation, **d** kurtosis, and **e** skewness values of v_e according to luminal A, luminal B, and triple-negative. *A* luminal A, *B* luminal B, *TN* triple-negative. The boxes show the median with the upper and lower quartiles. The whiskers indicate the minimal value within a 1.5 interquartile range (IQR) of the lower quartile, and the maximum value within a 1.5 IQR of the upper quartile. The open circles indicate the outliers. The horizontal bars show the significant differences between the subtypes. The *P* values above each plot were calculated with the Kruskal–Wallis test. The *P* values above each bar were calculated with the post hoc Steel–Dwass multiple comparison test

Discussion

In this study, we identified associations between DCE-MRI perfusion parameters and the pathologic prognostic factors and molecular subtypes of breast cancer and found that v_e showed better associations than did K^{trans} and k_{ep}.

The mean of v_e was significantly lower in breast cancers with high Ki-67 expression levels. Whereas some previous studies have reported that lower v_e values are significantly associated with the high histologic grade of breast cancers [6, 7], no reports have found an association with Ki-67 expression. v_e is defined as the volume of the EES space, which represents the amount of contrast agent that is temporarily trapped in the stromal space under DCE-MRI. Stromal tissue is known to interact closely with breast epithelial cells and plays a major role in tumor progression [18, 19]. Yim et al. observed that v_e values were lower in tumors with high cellularity [20]. High Ki-67 expression and mitotic index, an important component of histologic grade, of breast cancers are commonly recognized to represent greater tumor proliferative potential. Such tumors seem to have a high cellularity and small stromal space and may, consequently, show low v_e values.

TNBC lacks the expression of all three receptors (ER, PR, and HER2), and is known to have more aggressive histological features, clinical behaviors, and outcomes than luminal-type cancers. Recently, several studies of TNBC MRI features have been published. Morphologically, TNBC tends to present as a benign-like mass with a relatively circumscribed margin, which frequently shows rim enhancement and internal high-signal intensity on T2-weighted images [21–23]. Under functional imaging, TNBC shows a higher ADC on DWI because of a greater necrotic component [24, 25]. Through the quantitative analysis of DCE-MRI, several studies have observed significantly lower v_e values in TNBC with ROI placements that excluded areas of necrosis [7, 8, 26]. Lower v_e refers to TNBC with lower stromal space and tightly packed and highly cellular environments. In our study, the TNBC mean of v_e tended to be lower than that of the luminal type, although this difference was not statistically significant ($P = 0.068$). This discordance may be caused by intra- and inter-tumoral TNBC heterogeneities, under the small population ($n = 14$) of our study.

Regarding K^{trans} and k_{ep} values, several reports have investigated their relationships with prognostic factors and molecular subtypes of breast cancer [7, 8, 20, 26–28], although the conclusions, a few of which are inconsistent with our results, vary. K^{trans} reflects a combination of blood flow, vessel density, and permeability. Li et al. explained that any conditions that influence blood perfusion, such as cardia output and hypertension, which are difficult to control, might potentially confound measurements of K^{trans} [8]. On the hand, k_{ep} reflects only vessel permeability, and some reports [7, 8, 27] have shown correlations of higher k_{ep} with high histological or nuclear grade, ER negativity, high Ki-67 expression, and TNBC. However, one report has also shown that k_{ep} was not associated with any prognostic factors or molecular subtypes [28], which was similar to our results. The reason for this discrepancy is not clear; however, it may be related to differences in the study populations, MRI protocols, ROI placements, pharmacokinetic analysis software, and the substantial heterogeneity of breast cancers. Thus, further studies are needed to clarify these observations.

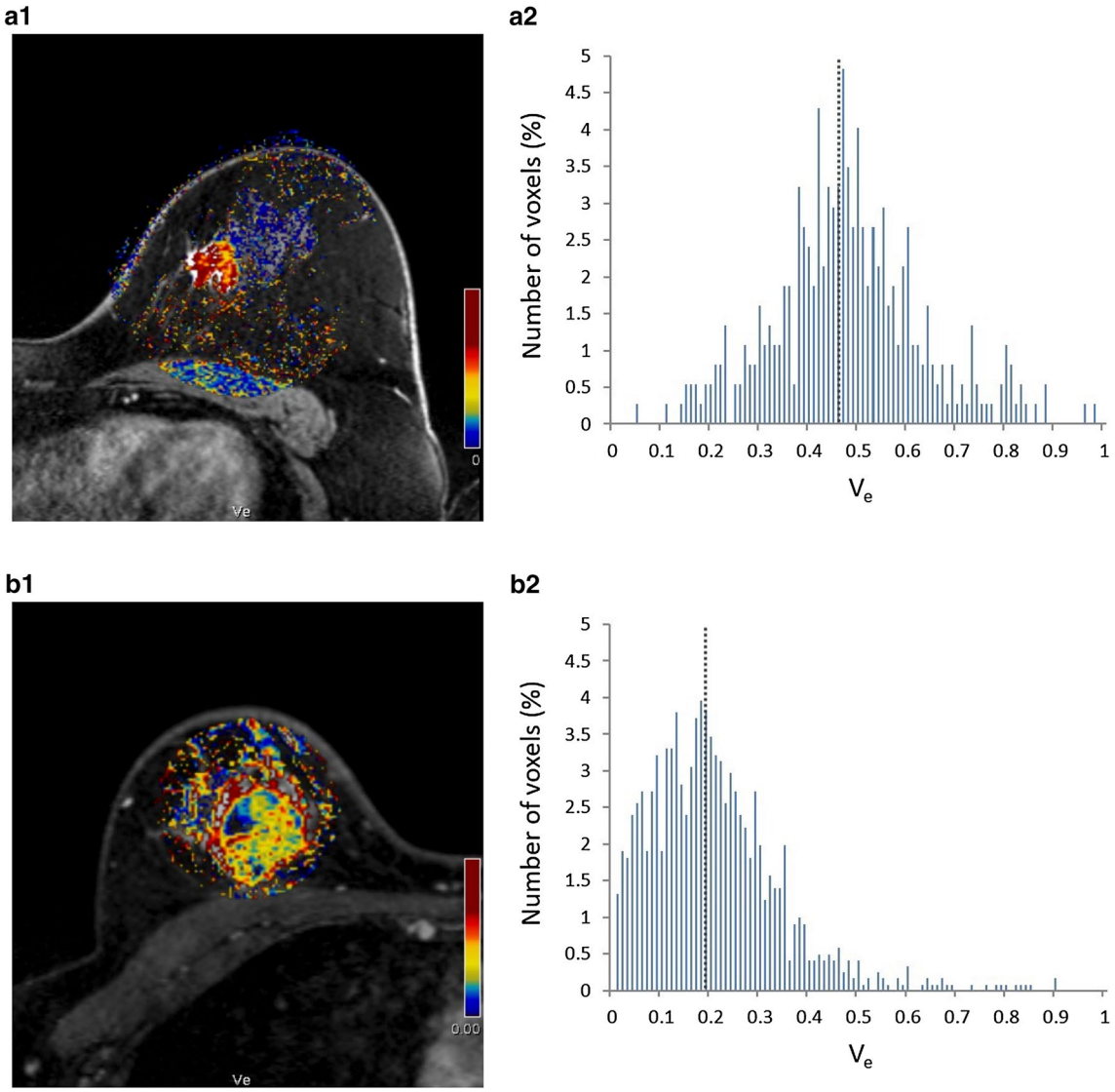

Fig. 4 **a** A 60-year-old woman with luminal A type cancer in the left breast [ER (+), PR (+), HER2 (−), Nuclear grade 1, Ki-67 10%]. The v_e color map (**a1**) and whole tumor histogram (**a2**) are shown. The mean, coefficient of variation, kurtosis, and skewness were 0.47, 0.32, 0.21, and 0.30, respectively. **b** A 34-year-old woman with triple-negative breast cancer in the right breast [ER (−), PR (−), HER2 (−), Nuclear grade 3, Ki-67 70%]. The v_e color map (**b1**) and whole tumor histogram (**b2**) are shown. The mean, coefficient of variation, kurtosis, and skewness were 0.20, 0.67, 3.61, and 1.43, respectively. The dotted line indicates the mean of the values

The most important finding of this study was that the coefficient of variation of v_e was significantly higher in cancers with ER negativity, high Ki-67 expression, and TNBC, which are considered aggressive and to have high proliferative activities. In addition, the skewness of v_e was significantly higher in cancers with high nuclear grade. Since we drew the ROIs to cover the entire tumor on the image of the slice with the largest diameter, the coefficient of variation, kurtosis, and skewness values were assumed to represent the intratumoral pharmacokinetic heterogeneity that reflects intratumoral angiogenesis and cellular density heterogeneities. Histologically, the distributions of stromal components, such as collagen fibrosis, cancer-associated fibroblast infiltration, and lymphocyte infiltration, can be also associated, because Yim et al. observed that the pharmacokinetic parameter values differed among breast cancer stromal types [20]. In histogram analysis, higher coefficient of variation indicates a more widely varying distribution of the data, higher kurtosis indicates a sharper peak and wider tails of the value distributions, and higher skewness indicates a shift of the data to the left, with an elongated tail on the right side (Fig. 4). Our result revealed that high proliferative breast cancers, such as TNBC, high Ki-67, and, high nuclear grade cancer, showed higher coefficient of variation, or skewness

of v_e values. The high proliferative capabilities of breast cancer are considered to be reflected in the high cell density regions, which show low v_e values, and in the heterogeneous and disproportional v_e parametric distributions, which reflect various microenvironments.

To the best of our knowledge, there are only two studies that have used histogram analyses to investigate the association of pharmacokinetic parameters with prognostic factors and molecular subtypes of breast cancers. These studies applied the 25th, median, and 75th percentile values, but not the coefficient of variation, kurtosis, and skewness values, and could not find correlative heterogeneity indices other than median K^{trans} or v_e [28, 29]. This is the first investigation using histogram analyses that could quantitatively correlate intratumoral pharmacokinetic heterogeneity with pathologic prognostic factors and molecular subtypes. Recently, "radiomics" or "radiogenomics," which refers to the high-throughput extraction of quantitative features and the use of analyses that are integrated with clinical and genomic data, is rapidly developing and gaining the interest of the medical community. One of the challenges for "radiomics" or "radiogenomics" in breast cancer is to create quantitative prognostic models that support evidence-based decision-making. Our results identify various v_e parameters that could possibly be utilized as MRI-derived biomarkers in future validations of radiomics to improve the predictive power for breast cancers and improve personalized managements.

Some notable limitations of our study should be kept in mind when interpreting these data. First, the number of patients was limited, especially patients with TNBC- and HER2-type cancer, which restrict statistical analyses. Second, we used two-dimensional ROIs that were drawn manually. The ROIs were chosen arbitrarily, and the reproducibility of the ROI designations was not assessed. As intratumoral heterogeneity can vary spatially and planarly, the values that were acquired from the two-dimensional ROIs may inadequately represent the heterogeneity. Third, we did not consider the location of heterogeneity. For example, texture analysis methods, such as gray-level co-occurrence matrix, gray-level run length matrix, and gray-level difference matrix, on DCE-MRI pharmacokinetic maps may represent intratumoral heterogeneity more accurately. Thibault et al. investigated the effectiveness of the texture analysis of voxel-based pharmacokinetic parametric maps for the early prediction of breast cancer therapy response [30]. Fourth, a daily protocol with a high spatial and limited temporal resolution of 60 s was used for DCE-MRI analysis. Heisen et al. concluded that, as temporal resolution decreases, K^{trans} becomes progressively underestimated (~4 to ~25%), and v_e becomes progressively overestimated (~1 to ~10%) [31]. The optimal temporal resolution seems to be less than 20 s for pharmacokinetic quantitative analysis of breast cancers [32]. On the other hand, regarding with prostate cancer, Othman et al. showed that there were no significant effects of temporal resolution (5 versus 30 s) on pharmacokinetic parameters [33]. There are no enough clearly supportive studies on pharmacokinetic analyses with low temporal resolution in breast cancers; however, several studies with limited daily protocol temporal resolution (71–84 s) have proven useful [9, 32, 34]. We consider that future studies with both high temporal and spatial resolution, using new technology such as compresses sensing, are desirable, and further studies are needed to determine optimal protocols that are compatible with pharmacokinetic and morphological assessments. Furthermore, we used the population-based AIF that was provided by the Tissue 4D software. If the individual AIF is measured accurately, then pharmacokinetic parameters can be calculated more accurately. However, the measured AIF is often poorly sampled in both clinical and preclinical MR systems because of the initial rapid increase in contrast agent concentration and the subsequent large-scale signal change that occurs in the arteries [35], which results in interobserver variability [36]. A population-based AIF can overcome the problems with high temporal resolution and ROI selection which are required for the measured AIF, and has been used when reliable AIFs from individual patients cannot be acquired. Finally, the estimated values of the pharmacokinetic parameters vary depending on the analysis software and pharmacokinetic model [37–39].

In conclusion, we found that various v_e parameters that we evaluated by a histogram analysis of DCE-MRI quantitatively correlated with breast cancer prognostic factors and molecular subtypes. Whole-lesion values of v_e, as well as distribution histogram parameters such as coefficient of variation and skewness, were associated with aggressiveness and high proliferative activities of breast cancer.

Compliance with ethical standards

Conflict of interest The authors declare that they have no conflict of interest.

References

1. Uzzan B, Nicolas P, Cucherat M, Perret GY. Microvessel density as a prognostic factor in women with breast cancer: a systematic review of the literature and meta-analysis. Cancer Res. 2004;64:2941–55.
2. Goede V, Fleckenstein G, Dietrich M, Osmers RG, Kuhn W, Augustin HG. Prognostic value of angiogenesis in mammary tumors. Anticancer Res. 1998;18:2199–202.
3. Weidner N, Folkman J, Pozza F, Bevilacqua P, Allred EN, Moore DH, et al. Tumor angiogenesis: a new significant and independent prognostic indicator in early-stage breast carcinoma. J Natl Cancer Inst. 1992;84:1875–87.
4. Cheng Z, Wu Z, Shi G, Yi Z, Xie M, Zeng W, et al. Discrimination between benign and malignant breast lesions using

volumetric quantitative dynamic contrast-enhanced MR imaging. Eur Radiol. 2017. https://doi.org/10.1007/s00330-017-5050-2.
5. El Khouli RH, Macura KJ, Kamel IR, Jacobs MA, Bluemke DA. 3-T dynamic contrast-enhanced MRI of the breast: pharmacokinetic parameters versus conventional kinetic curve analysis. AJR Am J Roentgenol. 2011;197:1498–505.
6. Yi B, Kang DK, Yoon D, Jung YS, Kim KS, Yim H, et al. Is there any correlation between model-based perfusion parameters and model-free parameters of time-signal intensity curve on dynamic contrast enhanced MRI in breast cancer patients? Eur Radiol. 2014;24:1089–96.
7. Koo HR, Cho N, Song IC, Kim H, Chang JM, Yi A, et al. Correlation of perfusion parameters on dynamic contrast-enhanced MRI with prognostic factors and subtypes of breast cancers. J Magn Reson Imaging. 2012;36:145–51.
8. Li SP, Padhani AR, Taylor NJ, Beresford MJ, Ah-See ML, Stirling JJ, et al. Vascular characterization of triple negative breast carcinomas using dynamic MRI. Eur Radiol. 2011;21:1364–73.
9. Drisis S, Metens T, Ignatiadis M, Stathopoulos K, Chao SL, Lemort M. Quantitative DCE-MRI for prediction of pathological complete response following neoadjuvant treatment for locally advanced breast cancer: the impact of breast cancer subtypes on the diagnostic accuracy. Eur Radiol. 2016;26:1474–84.
10. Aleskandarany MA, Vandenberghe ME, Marchiò C, Ellis IO, Sapino A, Rakha EA. Tumour heterogeneity of breast cancer: from morphology to personalised medicine. Pathobiology. 2018;85:23–34.
11. Heindl A, Sestak I, Naidoo K, Cuzick J, Dowsett M, Yuan Y. Relevance of spatial heterogeneity of immune infiltration for predicting risk of recurrence after endocrine therapy of ER + breast cancer. J Natl Cancer Inst. 2018;110:166–75.
12. Shin Y, Kim H, Han S, Won J, Jeong HE, Lee ES, et al. Extracellular matrix heterogeneity regulates three-dimensional morphologies of breast adenocarcinoma cell invasion. Adv Healthc Mater. 2013;2:790–4.
13. Choi Y, Kim SH, Youn IK, Kang BJ, Park WC, Lee A. Rim sign and histogram analysis of apparent diffusion coefficient values on diffusion-weighted MRI in triple-negative breast cancer: comparison with ER-positive subtype. PLoS One. 2017;12:e0177903.
14. Kim YJ, Kin SH, Lee AW, Jin MS, Kang BJ, Song BJ. Histogram analysis of apparent diffusion coefficients after neoadjuvant chemotherapy in breast cancer. Jpn J Radiol. 2016;34:657–66.
15. Kim JH, Ko ES, Lim Y, Lee KS, Han BK, Ko EY, et al. Breast cancer heterogeneity: MR imaging texture analysis and survival outcomes. Radiology. 2017;282:665–75.
16. Li Z, Ai T, Hu Y, Yan X, Nickel MD, Xu X, et al. Application of whole-lesion histogram analysis of pharmacokinetic parameters in dynamic contrast-enhanced MRI of breast lesions with the CAIPIRINHA-Dixon-TWIST-VIBE technique. J Magn Reson Imaging. 2018;47:91–6.
17. Tofts PS, Kermode AG. Measurement of the blood-brain barrier permeability and leakage space using dynamic MR imaging. 1. Fundamental concepts. Magn Reson Med. 1991;17:357–67.
18. Shekhar MP, Werdell J, Santner SJ, Pauley RJ, Tait L. Breast stroma plays a dominant regulatory role in breast epithelial growth and differentiation: implications for tumor development and progression. Cancer Res. 2001;61:1320–6.
19. Orimo A, Gupta PB, Sgroi DC, Arenzana-Seisdedos F, Delaunay T, Naeem R, et al. Stromal fibroblasts present in invasive human breast carcinomas promote tumor growth and angiogenesis through elevated SDF-1/CXCL12 secretion. Cell. 2005;121:335–48.
20. Yim H, Kang DK, Jung YS, Jeon GS, Kim TH. Analysis of kinetic curve and model-based perfusion parameters on dynamic contrast enhances MRI in breast cancer patients: correlations with dominant stroma type. Magn Reson Imaging. 2016;34:60–5.
21. Uematsu T, Kasami M, Yuen S. Triple-negative breast cancer: correlation between MR imaging and pathologic findings. Radiology. 2009;250:638–47.
22. Sung JS, Jochelson MS, Brennan S, Joo S, Wen YH, Moskowitz C, et al. MR imaging features of triple-negative breast cancers. Breast J. 2013;19:643–9.
23. Cho N. Molecular subtypes and imaging phenotypes of breast cancer. Ultrasonography. 2016;35:281–8.
24. Youk JH, Son EJ, Chung J, Kim JA, Kim EK. Triple-negative invasive breast cancer on dynamic contrast-enhanced and diffusion-weighted MR imaging: comparison with other breast cancer subtypes. Eur Radiol. 2012;22:1724–34.
25. Richard R, Thomassin I, Chapellier M, Scemama A, de Cremoux P, Varna M, et al. Diffusion-weighted MRI in pretreatment prediction of response to neoadjuvant chemotherapy in patients with breast cancer. Eur Radiol. 2013;23:2420–31.
26. An YS, Kang DK, Jung YS, Han S, Kim TH. Tumor metabolism and perfusion ratio assessed by 18F-FDG PET/CT and DCE-MRI in breast cancer patients: correlation with tumor subtype and histologic prognostic factors. Eur J Radiol. 2015;84:1365–70.
27. Kim JY, Kim SH, Kim YJ, Kang BJ, An YY, Lee AW, et al. Enhancement parameters on dynamic contrast enhanced breast MRI: do they correlate with prognostic factors and subtypes of breast cancers? Magn Reson Imaging. 2015;33:72–80.
28. Kim SH, Lee HS, Kang BJ, Song BJ, Kim HB, Lee H, et al. Dynamic contrast-enhanced mri perfusion parameters as imaging biomarkers of angiogenesis. PLoS One. 2016;11:e0168632.
29. Lee HS, Kim SH, Kang BJ, Baek JE, Song BJ. Perfusion parameters in dynamic contrast-enhanced MRI and apparent diffusion coefficient value in diffusion-weighted mri: association with prognostic factors in breast cancer. Acad Radiol. 2016;23:446–56.
30. Thibault G, Tudorica A, Afzal A, Chui SY, Naik A, Troxell ML, et al. DCE-MRI texture features for early prediction of breast cancer therapy response. Tomography. 2017;3:23–32.
31. Heisen M, Fan X, Buurman J, van Riel NA, Karczmar GS, ter Haar Romeny BM. The influence of temporal resolution in determining pharmacokinetic parameters from DCE-MRI data. Magn Reson Med. 2010;63:811–6.
32. de Bazelaire C, Calmon R, Thomassin I, Brunon C, Hamy AS, Fournier L, et al. Accuracy of perfusion MRI with high spatial but low temporal resolution to assess invasive breast cancer response to neoadjuvant chemotherapy: a retrospective study. BMC Cancer. 2011;11:361.
33. Othman AE, Falkner F, Weiss J, Kruck S, Grimm R, Martirosian P, et al. Effect of temporal resolution on diagnostic performance of dynamic contrast-enhanced magnetic resonance imaging of the prostate. Invest Radiol. 2016;51:290–6.
34. Park VY, Kim EK, Kim MJ, Yoon JH, Moon HJ. Perfusion parameters on breast dynamic contrast-enhanced MRI are associated with disease-specific survival in patients with triple-negative breast cancer. AJR Am J Roentgenol. 2017;208:687–94.
35. McGrath DM, Bradley DP, Tessier JL, Lacey T, Taylor CJ, Parker GJ. Comparison of model-based arterial input functions for dynamic contrast-enhanced MRI in tumor bearing rats. Magn Reson Med. 2009;61:1173–84.
36. Attenberger UI, Sourbron SP, Notohamiprodjo M, Lodemann KP, Glaser CG, Reiser MF, et al. MR-based semiautomated quantification of renal functional parameters with

a two-compartment model—an interobserver analysis. Eur J Radiol. 2008;65:59–65.
37. Othman AE, Falkner F, Kessler DE, Martirosian P, Weiss J, Kruck S, et al. Comparison of different population-averaged arterial-input-functions in dynamic contrast-enhanced MRI of the prostate: effects on pharmacokinetic parameters and their diagnostic performance. Magn Reson Imaging. 2016;34:496–501.
38. Heye T, Davenport MS, Horvath JJ, Feuerlein S, Breault SR, Bashir MR, et al. Reproducibility of dynamic contrast-enhanced MR imaging. Part I. Perfusion characteristics in the female pelvis by using multiple computer-aided diagnosis perfusion analysis solutions. Radiology. 2013;266:801–11.
39. Li X, Welch EB, Chakravarthy AB, Xu L, Arlinghaus LR, Farley J, et al. Statistical comparison of dynamic contrast-enhanced MRI pharmacokinetic models in human breast cancer. Magn Reson Med. 2012;68:261–71.